Immune-related molecular changes in the olfactory epithelium, structural alteration in the olfactory bulb, and psychosis

Kun Yang[1], Yuto Hasegawa[1], Jun Hua[2,9], Milan Dower[3], Semra Etyemez[1], Neal Prasad[1], Lauren Duvall[1], Adrian Paez[9], Amy Smith[7], Andrew P. Lane[7], Koko Ishizuka[1], Vidyulata Kamath[1], Atsushi Kamiya[1], and Akira Sawa[1,3,4,5,6,8]

Departments of Psychiatry[1], Radiology and Radiological Sciences[2],

Biomedical Engineering[3], Neuroscience[4], Phamarchology[5],

Genetic Medicine[6], and Otolaryngology-Head and Neck Surgery[7],

Johns Hopkins University School of Medicine, Baltimore, Maryland.

Departments of Mental Health[8],

Johns Hopkins Bloomberg School of Public Health, Baltimore, Maryland.

F.M. Kirby Research Center for Functional Brain Imaging[9], Kennedy Krieger Institute,

Baltimore, Maryland.

* Corresponding and contact author: Akira Sawa, asawa1@jhmi.edu

Abstract

Olfactory dysfunction has been reproducibly reported in patients with psychosis. Consistently, some studies have reported structural abnormalities in the olfactory bulb (OB) in psychotic disorders with modest sample size. Air pollution and viral infections in the upper respiratory tract, including those of SARS-CoV-2, are reportedly risk factors for brain dysfunction and mental disorders. These risk factors can disturb the olfactory epithelium (OE) that is connected with the OB via direct neuronal projections. Nevertheless, it is unknown whether and how a disturbance of the OE could possibly affect the structure of OB in the pathophysiological context of psychotic disorders. To address this knowledge gap, we first utilized an inducible OE inflammation mouse model (IOI model) and found that OE inflammation could induce a significant reduction in the OB volume, shrinkage of the glomerular layer and the external plexiform layer of OB, and decrease in the immunoreactivity of OMP (olfactory sensory neuron marker), Vglut2 (glutamatergic presynaptic marker), CCK8 (tufted cell marker), and PGP9.5 (mitral cell marker) in the glomerular layer of OB in IOI mice compared to control mice. We then analyzed 3 Tesla magnetic resonance imaging and molecular expression profiles of olfactory neuronal cells (ONCs) biopsied from living human subjects. Interestingly, we also observed a significant reduction in the OB volume, as well as alterations in the expression profiles in ONCs in first episode psychosis (FEP) patients compared to healthy controls. Higher expression levels of IOI immune genes (genes coding immune-related transcription factors up-regulated in IOI mice) in ONCs was significantly associated with smaller volumes of the OB in FEP patients. The subgroup of FEP patients with an up-regulation of IOI immune genes had significantly smaller OB volumes than other FEP patients. Together, our study implied the existence and connections between OE and OB pathologies in psychotic disorders.

Introduction

Deficits in olfactory function have been reproducibly reported in patients with psychotic disorders [1]. In these studies, three psychophysical measures (odor identification, odor discrimination, and odor detection threshold) have been frequently used [1–8]. Importantly, these deficits are observed in youths at-risk for psychosis [9–11]. Accordingly, olfactory dysfunction is also one of the key deficits in patients with first episode psychosis (FEP) [4,12–14]. Furthermore, olfactory deficits appear to predict poor outcomes in patients with schizophrenia and can identify patients at high risk of developing unremitting negative symptoms, particularly anhedonia [15,16].

Olfactory sensory neurons (OSNs) in the olfactory epithelium (OE) that are exposed to the nasal cavity receive odorants and project to glomeruli in the olfactory bulb (OB) where they form synapses on mitral and tufted cells [17]. Mitral and tufted cells then project to the primary olfactory cortex, where the information from OSNs is transmitted to the higher cortex, such as the orbitofrontal cortex and medial prefrontal cortex, as well as other central brain regions that are involved in emotion and cognition [18]. It is important to note that the external information perceived in the olfactory system can be transmitted with fewer synapses (only two, by bypassing the thalamus) to the central brain regions for emotion and cognition compared with other perceptions [19].

Deficits in the peripheral olfactory system (e.g., the OE and OB), or the central olfactory system, or both can elicit the aforementioned olfactory deficits [20]. Meanwhile, volumetric changes of the OB, mainly by magnetic resonance imaging (MRI) assessment, have been reported in multiple brain disorders [21–24]. A reduction in the OB volume has also been reported in psychiatric disorders, such as major depressive disorder and schizophrenia (SZ) [25–32]. Importantly, there are reports that indicate a volume reduction in subjects at high risk for psychosis [33,34], suggesting that

the changes found in SZ and related disorders may not be due to secondary effects of medication. More recently, SARS-CoV-2 infected patients with olfactory dysfunction have reportedly shown smaller OB volumes compared with healthy subjects [35], and a case report also indicated shrinkage of the OB in the course of SARS-CoV-2 infection [36].

Compared with many reports about the OB in brain disorders, much less literature is available on the biological assessment of the OE in psychotic disorders. Some studies were performed with postmortem OE, which include a seminal work by Arnold reporting a significant change in cell fate from stem cells to mature OSNs [37]. Some of these results, but not all, were reproduced by another group [38], which may be due to the heterogeneity of SZ pathophysiology [39]. An outstanding question is whether the pathological features observed in postmortem OE from chronic SZ patients may represent the signatures of a long-term compensation to the key pathological events when psychosis occurs and is active. Accordingly, it is important to conduct biological assessments of the OE freshly biopsied from patients with early-stage psychosis.

Air pollution has been highlighted as a major risk factor for SZ and related psychotic disorders [40–42], and can elicit pathological and immune/inflammatory responses in the OE at the biological levels [43]. Viral infection can also be a major adverse event for the OE that is exposed to the nasal cavity. Studies on herpes simplex virus and Alzheimer's Disease have suggested a link between viral infection in the nasal cavity and brain disorders [44–47]. More recently, intranasal infection with SARS-CoV-2 is underscored in the context of olfactory dysfunction, possibly followed by deficits in higher brain function and the development of psychosis [48,49]. These data suggest that peripheral olfactory system disturbances may underlie, as an important risk factor or driver, multiple neuropsychiatric disorders, including SZ and related psychotic disorders [50,51].

Nevertheless, the causal impact and underlying mechanism of peripheral olfactory pathology on brain disorders remain to be elucidated.

A recent basic science publication indicated that the stress response to induced inflammation in the OE could alter the cell fate of basal stem cells [horizontal basal stem cells (HBCs)] in an inducible OE inflammation mouse model (IOI model) [52]. The potential associations between nasal inflammation and OB have been suggested by preclinical studies [53–55]. On the other hand, our group has reported preliminary observations of a reduction of the OB volume derived from T1-weighted images at 3 Tesla in FEP patients (n=16) compared with healthy controls (n=22) [56]. Based on this background, we hypothesize that stress response in the OE may affect the structure of OB in the pathophysiological context of psychotic disorders. More specifically, we hypothesize that FEP patients, or at least a subset of FEP patients, may have immune-related molecular changes in the OE, associated with structural alteration in the OB. To address this hypothesis, we conducted both a preclinical study using the IOI model and a clinical study using OB volumes derived from T2-weighted images at 3 Tesla from 95 FEP patients and 89 healthy controls. We compared the structural changes in OB between IOI and control mice, and between FEP patients and healthy controls. Furthermore, we collected RNA sequencing (RNASeq) data from biopsied neuronal cells (olfactory neuronal cells, ONCs) from 45 FEP patients and 59 healthy controls (all these subjects had 3T MRI data). Studies showed that ONCs assemble the molecular profiles of neurons in the human brain and are particularly useful as surrogates of neuronal cells for studies of brain disorders in adolescence or young adulthood [57–61]. By utilizing this cell resource, we compared the expressional profiles between FEP patients and healthy controls and investigated the associations between the expression level of immune-related genes in ONCs and OB volume in FEP patients.

Materials and Methods

IOI mouse model

IOI mouse model was generated by crossing the Tet-response element (TRE)-TNF-α transgene mice with Cyp2g1-reverse tetracycline transactivator (rtTA) line and developed in the C57BL/6 background as previously described [62,52,63]. In this study, 3-4 month old IOI mice were treated with 0.2g/kg doxycycline (DOX) food for 6 weeks to induce TNF-α expression in the sustentacular cells of the OE, leading to chronic and local OE inflammation. Both male and female mice were used in each experiment by matching for sex and age. All animal procedures were approved by the Institutional Animal Care and Use Committee of Johns Hopkins University School of Medicine, and adhered to ethical considerations in animal research.

Immunohistochemistry and image analysis of mouse samples.

Immunohistochemistry was performed using our previously published methods with some modifications [64]. Mouse brains were extracted after perfusion with 4% paraformaldehyde (PFA). To measure the size of the OBs, we measured the length of the rostrocaudal axis between the top and baseline s of OBs, and the width at the middle along the OB length (**Figure 1A**). The fixed OBs and brains were embedded in cryocompound (Sakura Finetek USA, Torrance, CA, USA) after the replacement of PFA with 30% sucrose in phosphate-buffered saline (PBS). Coronal sections were obtained at 20 µm with a cryostat (Cat # CM 3050S, Leica, Buffalo Grove, IL, USA). The sections were heated in HistoVT One solution (Cat # 06380-05, Nacalai Tesque, Kyoto, Japan) for 30 min at 60 °C for antigen retrieval. The sections were then washed with PBS containing 0.5% Triton X-100, followed by blocking with 0.5% Triton X-100 and 1% normal goat serum for 1 h. The sections were washed with PBS containing 0.5% Triton X-100, then blocked with 0.5% Triton X-100 and 1% bovine skin gelatin for 1 h. After blocking, sections were incubated with primary antibodies [Goat anti-OMP antibody (Cat # 544-10001, Wako,

1:1000), Mouse anti-VGlut2 antibody (Cat # MAB5504, Sigma-Aldrich, 1:100), Rabbit anti-PGP9.5 antibody (Cat # NB300-676SS, NOVUS, 1:200), Rabbit anti-CCK8 antibody (Cat # C2581, Sigma-Aldrich, 1:500)] at 4 °C overnight. An additional incubation with secondary antibodies conjugated to Alexa 488 (Cat # A-21206, Invitrogen, 1:400), Alexa 568 (Cat # A-32773, Invitrogen, 1:400), Alexa 647 (Cat # A-32849, Invitrogen, 1:400) was performed for 2 h. Nuclei were labeled with DAPI (Cat # 10236276001, Roche, Indianapolis, IN, USA). Immunofluorescence images were acquired using the Zeiss LSM700 confocal microscope with ZEN 2010 software (Carl Zeiss, Thornwood, New York, USA). To assess the area of the layers in the OB, the middle section was selected and divided into each layer by using the DAPI signal. The area of each layer was measured separately by using ImageJ-FIJI software (https://imagej.net/Fiji). The proportion of each layer was determined by dividing the area of each layer by the total OB area. To measure signal intensity, we created a 2D mask of the affected area and determined the mean fluorescence of the signal in all sections using ImageJ-FIJI software (https://imagej.net/Fiji). Identical parameters for all imaging and threshold settings were used for all groups to minimize experimental bias.

Human study participants

This study was conducted in accordance with The Code of Ethics of the World Medical Association (1964 Declaration of Helsinki) and was approved by the Johns Hopkins School of Medicine Institutional Review Board. Written informed consent was obtained for all participants. Adolescents and young adults between 18 and 35 years old were recruited from within and outside of the Johns Hopkins Hospital. Exclusion criteria included history of traumatic brain injury, neurologic condition, intellectual disability, cancer, viral infection, active substance abuse, and conditions affecting olfaction (e.g, history of sinus surgery, rhinoplasty, chronic rhinosinusitis). Controls were screened and excluded for a family history of psychotic disorders.

Patients must be within 24 months of the onset of psychotic manifestations as assessed by study team psychiatrists using the Structured Clinical Interview for DSM-IV (SCID) and information from available medical records.

The present study investigated the data from 89 healthy controls and 95 FEP patients. Patients were diagnosed with SZ (*n* = 50), schizoaffective disorder (*n* = 10), schizophreniform disorder (n=3), bipolar disorder with psychosis (*n* = 21), major depressive disorder with psychosis (*n* = 5), substance-induced psychosis (*n* = 2), brief psychotic disorder (n=2), and psychotic disorder not otherwise specified (n=2). The majority of patients, except five patients, were medicated. Antipsychotic medication dosages were converted to chlorpromazine (CPZ) equivalents using published reference tables with the Defined Daily Doses (DDDs) method [65].

3T MRI scans and OB volume measurement

All images were acquired on a 3T Philips MRI scanner (Philips Healthcare, Best, The Netherlands). The three-dimensional, T2-weighted, magnetization-prepared rapid acquisition with gradient echo (MPRAGE) scan was acquired for each participant with the following parameters: 1mm isotropic voxel, repetition time (TR) = 8.1 ms, echo time (TE) = 3.7 ms, flip angle = 8°, field of view (FOV) = 256mm x 256mm x 170mm, 170 slices, duration = 4 min 16 sec.

The FMRIB Software Library (FSL, https://fsl.fmrib.ox.ac.uk/fsl/) software was used to normalize the T2-weighted MPRAGE images into the MNI space. Subsequent analysis was performed in Insight ToolKitSNAP (ITK-SNAP) (www.itksnap.org). The OB was manually identified and segmented on coronal images, with additional corrections made in the sagittal and axial planes. Volumetric measures were obtained using the built-in functions in ITK-SNAP at the

level of the anterior cribriform plate following the procedures established previously [32]. Two experienced researchers (NP and LD) performed the segmentation separately and were blinded to participant information. After all segmentation was completed, discrepancies between the two researchers were assessed and final measurements were agreed upon. The intraclass correlation coefficient for inter-rater reliability between raters (NP and LD) was 0.86.

ONCs obtained via nasal biopsy

The nasal biopsy was conducted at the Johns Hopkins Otolaryngology Clinic. The biopsy procedure was described previously [59,66]. ONCs were enriched from nasal biopsied tissue as follows: First, biopsied tissues were incubated with 2.4 U/mL Dispase II for 45 min at 37ºC, and mechanically minced into small pieces. Then, the tissue pieces were further treated with 0.25 mg/mL collagenase A for 10 min at 37ºC. Dissociated cells were gently suspended, and centrifuged to obtain pellets. Cell pellets were resuspended in DMEM/F12 supplemented with 10% FBS and antibiotics (D-MEM/F12 medium) and tissue debris was removed by transferring only the cell suspension into a new tube. Cells from the suspension were then plated on 6-well plates in fresh D-MEM/F12 medium (Day 0 plate). Cells floating were collected at days 2 (Day 2 plate) and day 7 (Day 7 plate), and further incubated on 6-well plates. Through these processes, connective tissue-origin cells and non-neuronal cells that are attached in Day 0 and 2 plates were removed. Accordingly, we examined cells in Day 7 plate as ONCs under the hypothesis that these are neuronal and homogeneous in the present study. ONCs were stored in liquid nitrogen tanks until further experiments, in which ONCs were recovered and cultured in the D-MEM/F12 medium with the media change every 2-3 days. In summary, without any genetic and chemical reprogramming and conversion, we enriched the neuronal cell population [58,67].

Molecular expression profiles (RNASeq) of ONCs

Total RNA was isolated from ONCs using the RNeasy Plus Mini Kit (Qiagen). RNA quality was assessed on the Agilent Fragment Analyzer using an RNA High Sensitivity (DNF-472) and quantified using a Qubit 4 RNA BR kit (Thermo Fisher). RNA libraries were prepared with 500 ng total RNA. Library generation was accomplished using the NEBNext Ultra II Directional RNA Library Prep Kit for Illumina (E7760 and E7490) following the NEBNext Poly(A) mRNA Magnetic Isolation Module protocol. Libraries were enriched using 11 cycles of PCR amplification. Library quality and quantification was assessed on the Agilent Fragment Analyzer using a High Sensitivity NGS Kit (DNF-474) and a Qubit 4 RNA BR kit (Thermo Fisher). Samples were then normalized to 4 nM and pooled in equimolar amounts. Paired-End Sequencing was performed using Illumina's NovaSeq6000 S4 200 cycle kit.

FastQC [68] was used to check the quality of reads. High-quality data were obtained from raw data by using cutadapt [69] to remove adapters, primers, and reads with low quality (option -q 10) or shorter than 20 nt. Hisat2 (option --dta) [70] was used to map the clean reads to the human genome, version GRCh38 (Genome Reference Consortium Human Build 38). Stringtie [70] was used to assemble and merge transcripts and estimate transcript abundance. A Python script (prepDE.py) provided by the Stringtie developer [70] was used to create count tables for further analysis.

Statistical analysis

R version 4.1.2 was used to conduct statistical analysis. For the preclinical study, t-test was conducted to compare data between IOI mice and control mice

For the clinical study, t-test and chi-squared test were conducted to compare demographics between groups for continuous and categorical variables, respectively. Analysis of covariance (ANCOVA) with age, sex, race, tobacco usage status (Yes/No), and intracranial volume as covariates was performed to compare the total, left, and right OB volumes between FEP patients and healthy controls. Differential expression analysis was performed to compare the expressional profiles between FEP patients and healthy controls using R library *DESeq2* [71]. Age, sex, race, tobacco usage status (Yes/No), and one hidden/unknown confounding factor identified by *sva* [72] were included as covariates in the design formula. The Benjamini and Hochberg procedure was used for multiple comparison correction. Genes with false discovery rates (FDR) smaller than 0.05 were considered significant. Gene set enrichment analysis (GSEA) [73] (the GSEAPreranked module was used and pathways with less than 10 genes or more than 500 genes were excluded) on the Reactome Pathway Database [74] was conducted to identify molecular pathways altered in FEP patients compared with healthy controls. Pathways with FDRs smaller than 0.05 were considered significant.

Enrichment analysis was performed to examine whether risk genes for brain-disorder-related traits and immune-related traits identified by genome-wide association studies (GWAS) were over-represented in differentially expressed genes (FDR < 0.05) in FEP patients compared with healthy controls, respectively. The NHGRI-EBI GWAS Catalog [75] was used to identify risk genes. Traits with an immune response as the core mechanism or symptom were selected as immune-related traits (**Table S1**). Brain-disorder-related traits included SZ (EFO id: MONDO_0005090), bipolar disorder (EFO id: EFO_0000289), psychosis (EFO id: EFO_0005407), Alzheimer's disease (EFO id: MONDO_0004975), Parkinson's disease (EFO id: MONDO_0005180), and dementia (EFO id: HP_0000726). Genes with p-values smaller than

1E-8 and an odd ratio larger than 1 from the GWAS were considered as risk genes. Over-representation was assessed using a chi-square test for the following 2×2 contingency table:

	Risk Gene	Not Risk Gene
differentially expressed genes		
Not differentially expressed genes		

Partial correlation analysis controlling for age, sex, race, tobacco usage status (Yes/No), intracranial volume, CPZ dose, and duration of illness was performed to evaluate the correlation between gene expression and OB volume in FEP patients. Genes with low expression levels [Transcripts Per Million (TPM) less than 0.1 in more than 30% of the total samples] were excluded from the analysis. GSEA with the same parameters as mentioned above was conducted to identify molecular pathways overprinted in genes correlated with OB volumes. Power analysis was conducted to estimate the sample size for reaching a power of 0.8 at the significance level of 3.42E-06 (0.05 / the number of genes expressed in ONCs) for testing the correlations between individual gene expression and OB volumes.

In addition to the above unbiased genome-wide analysis, we also evaluated the correlation between the expression of IOI immune genes (genes coding immune-related transcription factors up-regulated in IOI mice, reported in supplemental table 4 by Chen et al. [52]) in ONCs and OB volume in FEP patients. Principal component analysis was conducted to reduce the dimension of expressional profiles of IOI immune genes. The first principal component was used as an indicator of the overall expressional levels of IOI immune genes. Partial correlation analysis controlling for age, sex, race, tobacco usage status (Yes/No), intracranial volume, CPZ dose, and duration of illness was performed to evaluate the association between the overall expressional levels of IOI immune genes and OB volume in FEP patients.

Results

Structural alterations in OB induced by OE inflammation in IOI mice

We examined the impact of OE inflammation on the OB volume and structure in adult male and female mice. Mice were fed a DOX-containing diet (IOI mice) or a non-DOX-containing diet (control mice) for 6 weeks. Upon completion of the OE inflammation-inducing process, we found reductions in the length (p-value = 9.87E-03) and width (p-value = 3.65E-03) of OB in IOI mice compared with the control mice (**Figure 1A**). We next examined the effect of OE inflammation on the layered structure of OB by measuring the area enclosed by the boundaries of each layer in the coronal sections from the middle of OB. The glomerular layer (p-value = 1.18E-07) and external plexiform layer (p-value = 3.30E-05) in IOI mice were smaller than those in the control mice, whereas no significant differences were observed in the mitral cell layer plus the internal plexiform layer (p-value = 0.98) or granule cell layer (p-value = 0.68) (**Figure 1B**).

Immunohistochemical experiments revealed that OE inflammation reduced the signal intensity of OMP (mature OSNs marker), Vglut2 (glutamatergic pre-synapse marker), CCK8 (tufted cell marker), and PGP9.5 (mitral cell marker) in the glomerular layer (**Figure 1C**). These results suggested that OE inflammation could impair direct synaptic inputs from OSNs to OB projection neurons.

Volumetric alterations in OB in FEP patients

To investigate whether the association between olfactory inflammation and OB structure is related to psychosis, we collected T2-weighted images at 3 Tesla and measured the OB volume from 95 FEP patients and 89 healthy controls (**Figure 2A**). The demographic summary of study participants is listed in **Table 1**. FEP patients had younger age and more percentage of males, Caucasians, and tobacco users. Through ANCOVA with age, sex, race, tobacco usage status

(Yes/No), and intracranial volume as covariates, we observed a significant reduction in the volume of the total (p-value = 1.99E-04), right (p-value = 5.57E-04), and left (p-value = 7.08E-04) in FEP patients compared with healthy controls (**Figure 2B-D**). This result implied the existence of OB pathology (disease-related structural changes in OB) in FEP.

Genome-wide analysis: alterations in gene expressional profiles in ONCs in FEP patients and their associations with OB volume

We next examined the expressional alterations in ONCs in FEP patients compared with healthy controls. Among 95 FEP patients and 89 healthy controls who had OB volume data, we collected ONCs from 45 FEP patients and 59 healthy controls and obtained RNA-Seq data. Differential expression analysis identified 35 significant genes in FEP patients (**Table S2**) compared with healthy controls after controlling for confounding factors and multiple comparison correction (see **Methods**). Enrichment analysis found that risk genes for brain disorders (p-value = 0.01) and immune-related disorders (p-value = 0.02) were significantly overrepresented in these 35 significant genes. Further GSEA analysis of genome-wide genes ranked by their effect size from differential expression analysis identified 237 significant pathways, among which, 17 pathways belonged to the Reactome Immune System catalog (**Table S3**). This result implied the existence of OE pathology (disease-related molecular changes in OE) in FEP, which included pathological changes in immune-related molecular changes.

We further tested whether there was an association between the OB and OE pathologies in FEP patients. Genome-wide partial correlation analysis controlling for confounding factors didn’t identify any gene with a significant correlation with OB volumes after multiple comparison correction, because the effect sizes of individual genes were small. Power analysis showed that a larger sample size (137 FEP patients) is needed to reach a power of 0.8. On the other hand,

GSEA analysis of genome-wide genes ranked by their effect size from correlation analysis identified 31, 175, and 17 significant pathways associated with total, right, and left OB volumes after multiple comparison correction, respectively. Interestingly, 4 pathways belonging to the Reactome Immune System catalog were significantly enriched in genes altered in FEP patients and also in genes correlated with the right OB volume in FEP patients. These 4 pathways are: NIK/NF-kB signaling (R-HSA-5676590), dectin-1 mediated NF-kB signaling (R-HSA-5607761), antigen processing-cross presentation (R-HSA-1236978), and interferon-stimulated gene 15 in antiviral immunity (R-HSA-1169408)

Integrative analysis of preclinical and clinical data: associations between immune-related molecular changes in ONCs and OB volume in FEP patients

One uniqueness of this study is that we employed both preclinical and clinical data to test our hypothesis. A previous study has identified immune-related transcription factors that were up-regulated in HBCs of IOI mice (referred to as IOI immune genes in short) compared with control mice [52]. In addition, our study of single-cell RNA-Seq profiles of ONCs showed that ONCs and HBCs had the highest similarity among other cell types in OE. Therefore, we hypothesize that the up-regulation of IOI immune genes in ONCs may be associated with the reduction in OB volumes in FEP patients. Partial correlation analysis controlling for confounding factors was conducted to test the correlation between OB volumes and the overall expression levels of IOI immune genes (the first principal component). Consistent with our hypothesis, we observed negative correlations in IOI immune genes expression levels with total (p-value = 0.08), right (p-value = 0.04), and left (p-value = 0.22) OB volumes, where the correlation with right OB volume was statistically significant (**Figure 3**). Furthermore, we compared the top 10% of FEP patients with up-regulation in IOI immune genes with the remaining FEP patients. Interestingly, the

subgroup of FEP with up-regulated IOI immune genes had smaller OB volumes than other FEP patients (**Figure S1**).

Discussion

Here we reported an integrative study of preclinical and clinical data with the aim to explore the associations among immune-related molecular changes in the OE, structural alteration in the OB, and psychosis. Our preclinical study found that IOI mice had a significant reduction in the OB volume, shrinkage of the glomerular layer and the external plexiform layer of OB, and a decrease in the immunoreactivity of markers for OSNs and principal OB projection neurons such as tufted and mitral cells, compared with control mice, which suggested that OE inflammation could cause structural alterations in OB. On the other hand, our clinical study identified a significant reduction in the OB volume in FEP patients, which is consistent with the findings from multiple groups [25,28,32], but our cohort had a much larger sample size. Most importantly, we utilized ONCs, biopsied neuronal cells from living subjects, in this study. We observed alterations in gene expression profiles in ONCs in FEP patients compared with healthy controls, suggesting the existence of OE pathology in FEP. The unbiased whole-genome analysis further highlighted several immune-related pathways including those related to NF-kB pathways with altered expressional levels in FEP patients, as well as associations with the OB volume changes in FEP patients. Consistently, a previous preclinical study has also underscored NF-kB pathway as one of the pathways which were significantly altered by OE inflammation[52]. To further investigate the association between the expression of immune-related gene in OE and OB volume, we integrated the observations from the preclinical study with clinical data and found that the upregulation of IOI immune genes in ONCs was significantly associated with the reduction of OB volume in FEP patients. The subgroup of FEP patients with upregulation of IOI immune genes had significantly smaller OB volumes than other FEP patients. Together, our study

suggested the existence of OE and OB pathologies in FEP patients, and the potential role of the mechanistic link between OE and OB pathologies in psychotic disorders.

Possible OE pathology in psychotic disorders have been suggested [37,76–78]. Nevertheless, the data in classic neuropathology have not been perfectly consistent [37,38], partly because of biological heterogeneity in the same diagnostic criteria. Several studies addressed possible molecular changes in postmortem OE, but all of them took, to the best of our knowledge, a candidate molecular approach and studied only a limited number of molecules [77,78]. More fundamentally, although all these postmortem OE studies are informative, it is important to figure out whether the pathological features observed in postmortem OE may represent the signatures of long-term compensation to the key pathological events when psychosis occurs and is active. Accordingly, the use of biopsied OE samples for biological assessment has recently become active. Investigators have applied comprehensive molecular approaches, including unbiased RNA-seq and proteomic assessments, to neuronal cell cultures originating from biopsied OE, and reported significant, pathological changes at the molecular level [57,67,79–81,81–89]. Nevertheless, these excellent studies with OE-derived neuronal cells were not directly linked to the data of olfactory neurocircuitry. In this sense, the present study provides a new avenue for studying OE pathology in association with the OB volume, which is expected to affect the higher cortex.

Future studies may include investigating a relationship among adverse events in the nasal cavity, OE pathology at both the histological and molecular levels, structural/functional brain imaging data of the OB and upper neurocircuitry, as well as clinical phenotypes, including olfactory functional changes. To define cell-type specificity in a molecular study of the OE, the introduction of spatial transcriptomics (although ONCs may represent profiles of progenitor cells) [90] may also open a new window for psychosis research.

Acknowledgements

This study is supported by the National Institutes of Mental Health Grants MH-092443 (to AS), MH-094268 (to AS, AK), MH-105660 (to AS), and MH-107730 (to AS); foundation grants from Stanley (to AS), RUSK/S-R (to AS), a NARSAD young investigator award from Brain and Behavior Research Foundation (to AS, KY), NS-108452 (to JH, VK), AG-064093 (to JH, VK), DA-041208 (to AK), AG-065168 (to AK), DC-016106 (to AL), and AI-132590 (to AL)

The authors wish to extend their gratitude to the participants in the current study. The authors appreciate Ms. Yukiko Lema for research management and manuscript organization.

References

1 Moberg PJ, Kamath V, Marchetto DM, Calkins ME, Doty RL, Hahn C-G *et al.* Meta-analysis of olfactory function in schizophrenia, first-degree family members, and youths at-risk for psychosis. *Schizophr Bull* 2014; **40**: 50–59.

2 Cohen AS, Brown LA, Auster TL. Olfaction, 'olfiction,' and the schizophrenia-spectrum: an updated meta-analysis on identification and acuity. *Schizophr Res* 2012; **135**: 152–157.

3 Ishizuka K, Tajinda K, Colantuoni C, Morita M, Winicki J, Le C *et al.* Negative symptoms of schizophrenia correlate with impairment on the University of Pennsylvania smell identification test. *Neurosci Res* 2010; **66**: 106–110.

4 Kamath V, Lasutschinkow P, Ishizuka K, Sawa A. Olfactory Functioning in First-Episode Psychosis. *Schizophr Bull* 2018; **44**: 672–680.

5 Kiparizoska S, Ikuta T. Disrupted Olfactory Integration in Schizophrenia: Functional Connectivity Study. *Int J Neuropsychopharmacol* 2017; **20**: 740–746.

6 Kopala LC, Good K, Honer WG. Olfactory identification ability in pre- and postmenopausal women with schizophrenia. *Biol Psychiatry* 1995; **38**: 57–63.

7 Malaspina D, Wray AD, Friedman JH, Amador X, Yale S, Hasan A *et al.* Odor discrimination deficits in schizophrenia: association with eye movement dysfunction. *J Neuropsychiatry Clin Neurosci* 1994; **6**: 273–278.

8 Turetsky BI, Hahn C-G, Borgmann-Winter K, Moberg PJ. Scents and nonsense: olfactory dysfunction in schizophrenia. *Schizophr Bull* 2009; **35**: 1117–1131.

9 Brewer WJ, Wood SJ, McGorry PD, Francey SM, Phillips LJ, Yung AR *et al.* Impairment of olfactory identification ability in individuals at ultra-high risk for psychosis who later develop schizophrenia. *Am J Psychiatry* 2003; **160**: 1790–1794.

10 Kotlicka-Antczak M, Pawełczyk A, Karbownik MS, Pawełczyk T, Strzelecki D, Żurner N *et al.* Deficits in the identification of pleasant odors predict the transition of an at-risk mental state to psychosis. *Schizophr Res* 2017; **181**: 49–54.

11 Woodberry KA, Seidman LJ, Giuliano AJ, Verdi MB, Cook WL, McFarlane WR. Neuropsychological profiles in individuals at clinical high risk for psychosis: relationship to psychosis and intelligence. *Schizophr Res* 2010; **123**: 188–198.

12 Chen X, Xu J, Li B, Guo W, Zhang J, Hu J. Olfactory impairment in first-episode schizophrenia: a case-control study, and sex dimorphism in the relationship between olfactory impairment and psychotic symptoms. *BMC Psychiatry* 2018; **18**: 199.

13 Kamath V, Crawford J, DuBois S, Nucifora FC, Nestadt G, Sawa A *et al.* Contributions of olfactory and neuropsychological assessment to the diagnosis of first-episode schizophrenia. *Neuropsychology* 2019; **33**: 203–211.

14 Kamath V, Turetsky BI, Calkins ME, Kohler CG, Conroy CG, Borgmann-Winter K *et al.* Olfactory processing in schizophrenia, non-ill first-degree family members, and young

people at-risk for psychosis. *World J Biol Psychiatry Off J World Fed Soc Biol Psychiatry* 2014; **15**: 209–218.

15 Good KP, Tibbo P, Milliken H, Whitehorn D, Alexiadis M, Robertson N *et al.* An investigation of a possible relationship between olfactory identification deficits at first episode and four-year outcomes in patients with psychosis. *Schizophr Res* 2010; **124**: 60–65.

16 Lin A, Brewer WJ, Yung AR, Nelson B, Pantelis C, Wood SJ. Olfactory identification deficits at identification as ultra-high risk for psychosis are associated with poor functional outcome. *Schizophr Res* 2015; **161**: 156–162.

17 Mori K, Sakano H. How is the olfactory map formed and interpreted in the mammalian brain? *Annu Rev Neurosci* 2011; **34**: 467–499.

18 Mori K, Sakano H. Olfactory Circuitry and Behavioral Decisions. *Annu Rev Physiol* 2021; **83**: 231–256.

19 Su C-Y, Menuz K, Carlson JR. Olfactory perception: receptors, cells, and circuits. *Cell* 2009; **139**: 45–59.

20 Sawa A, Cascella NG. Peripheral olfactory system for clinical and basic psychiatry: a promising entry point to the mystery of brain mechanism and biomarker identification in schizophrenia. *Am J Psychiatry* 2009; **166**: 137–139.

21 Chen S, Tan H, Wu Z, Sun C, He J, Li X *et al.* Imaging of olfactory bulb and gray matter volumes in brain areas associated with olfactory function in patients with Parkinson's disease and multiple system atrophy. *Eur J Radiol* 2014; **83**: 564–570.

22 Chen B, Zhong X, Mai N, Peng Q, Wu Z, Ouyang C *et al.* Cognitive Impairment and Structural Abnormalities in Late Life Depression with Olfactory Identification Impairment: an Alzheimer's Disease-Like Pattern. *Int J Neuropsychopharmacol* 2018; **21**: 640–648.

23 Li J, Gu C-Z, Su J-B, Zhu L-H, Zhou Y, Huang H-Y *et al.* Changes in Olfactory Bulb Volume in Parkinson's Disease: A Systematic Review and Meta-Analysis. *PloS One* 2016; **11**: e0149286.

24 Petekkaya E, Kaptan Z, Unalmis D, Burakgazi G, Kus B, Melek IM *et al.* An investigation of olfactory bulb and entorhinal cortex volumes in both patients with Alzheimer's disease and healthy individuals, and a comparative analysis of neuropeptides. *Med Science* 2020; **9**: 866–871.

25 Asal N, Bayar Muluk N, Inal M, Şahan MH, Doğan A, Buturak SV. Olfactory bulbus volume and olfactory sulcus depth in psychotic patients and patients with anxiety disorder/depression. *Eur Arch Oto-Rhino-Laryngol Off J Eur Fed Oto-Rhino-Laryngol Soc EUFOS Affil Ger Soc Oto-Rhino-Laryngol - Head Neck Surg* 2018; **275**: 3017–3024.

26 Gul AI, Sari K, Ozkiris M, Aydin R, Simsek GG, Serin HI *et al.* Correlation Between Olfactory Bulb Volume and Chronic Depression: A Magnetic Resonance Imaging Study. *Klin Psikofarmakol Bül-Bull Clin Psychopharmacol* 2015; **25**: 280–286.

27 Negoias S, Croy I, Gerber J, Puschmann S, Petrowski K, Joraschky P *et al.* Reduced olfactory bulb volume and olfactory sensitivity in patients with acute major depression. *Neuroscience* 2010; **169**: 415–421.

28 Nguyen AD, Pelavin PE, Shenton ME, Chilakamarri P, McCarley RW, Nestor PG *et al.* Olfactory sulcal depth and olfactory bulb volume in patients with schizophrenia: an MRI study. *Brain Imaging Behav* 2011; **5**: 252–261.

29 Rottstädt F, Han P, Weidner K, Schellong J, Wolff-Stephan S, Strauß T *et al.* Reduced olfactory bulb volume in depression-A structural moderator analysis. *Hum Brain Mapp* 2018; **39**: 2573–2582.

30 Rottstaedt F, Weidner K, Hummel T, Croy I. Pre-aging of the Olfactory Bulb in Major Depression With High Comorbidity of Mental Disorders. *Front Aging Neurosci* 2018; **10**: 354.

31 Rottstaedt F, Weidner K, Strauß T, Schellong J, Kitzler H, Wolff-Stephan S *et al.* Size matters - The olfactory bulb as a marker for depression. *J Affect Disord* 2018; **229**: 193–198.

32 Turetsky BI, Moberg PJ, Yousem DM, Doty RL, Arnold SE, Gur RE. Reduced olfactory bulb volume in patients with schizophrenia. *Am J Psychiatry* 2000; **157**: 828–830.

33 Turetsky BI, Moberg PJ, Quarmley M, Dress E, Calkins ME, Ruparel K *et al.* Structural anomalies of the peripheral olfactory system in psychosis high-risk subjects. *Schizophr Res* 2018; **195**: 197–205.

34 Turetsky BI, Moberg PJ, Arnold SE, Doty RL, Gur RE. Low olfactory bulb volume in first-degree relatives of patients with schizophrenia. *Am J Psychiatry* 2003; **160**: 703–708.

35 Kandemirli SG, Altundag A, Yildirim D, Tekcan Sanli DE, Saatci O. Olfactory Bulb MRI and Paranasal Sinus CT Findings in Persistent COVID-19 Anosmia. *Acad Radiol* 2021; **28**: 28–35.

36 Chiu A, Fischbein N, Wintermark M, Zaharchuk G, Yun PT, Zeineh M. COVID-19-induced anosmia associated with olfactory bulb atrophy. *Neuroradiology* 2021; **63**: 147–148.

37 Arnold SE, Han LY, Moberg PJ, Turetsky BI, Gur RE, Trojanowski JQ *et al.* Dysregulation of olfactory receptor neuron lineage in schizophrenia. *Arch Gen Psychiatry* 2001; **58**: 829–835.

38 Minovi A, Dombrowski T, Brüne M, Dazert S, Juckel G. Olfactory function and morphology of olfactory epithelium in an adult population with schizophrenia. *Schizophr Res* 2015; **161**: 513–514.

39 Owen MJ, Sawa A, Mortensen PB. Schizophrenia. *Lancet Lond Engl* 2016; **388**: 86–97.

40 Gao Q, Xu Q, Guo X, Fan H, Zhu H. Particulate matter air pollution associated with hospital admissions for mental disorders: A time-series study in Beijing, China. *Eur Psychiatry J Assoc Eur Psychiatr* 2017; **44**: 68–75.

41 Newbury JB, Arseneault L, Beevers S, Kitwiroon N, Roberts S, Pariante CM *et al.* Association of Air Pollution Exposure With Psychotic Experiences During Adolescence. *JAMA Psychiatry* 2019; **76**: 614–623.

42 Pedersen CB, Raaschou-Nielsen O, Hertel O, Mortensen PB. Air pollution from traffic and schizophrenia risk. *Schizophr Res* 2004; **66**: 83–85.

43 Ajmani GS, Suh HH, Pinto JM. Effects of Ambient Air Pollution Exposure on Olfaction: A Review. *Environ Health Perspect* 2016; **124**: 1683–1693.

44 Eimer WA, Vijaya Kumar DK, Navalpur Shanmugam NK, Rodriguez AS, Mitchell T, Washicosky KJ *et al.* Alzheimer's Disease-Associated β-Amyloid Is Rapidly Seeded by Herpesviridae to Protect against Brain Infection. *Neuron* 2018; **99**: 56-63.e3.

45 Itzhaki RF, Golde TE, Heneka MT, Readhead B. Do infections have a role in the pathogenesis of Alzheimer disease? *Nat Rev Neurol* 2020; **16**: 193–197.

46 Itzhaki RF, Lathe R, Balin BJ, Ball MJ, Bearer EL, Braak H *et al.* Microbes and Alzheimer's Disease. *J Alzheimers Dis JAD* 2016; **51**: 979–984.

47 Readhead B, Haure-Mirande J-V, Funk CC, Richards MA, Shannon P, Haroutunian V *et al.* Multiscale Analysis of Independent Alzheimer's Cohorts Finds Disruption of Molecular, Genetic, and Clinical Networks by Human Herpesvirus. *Neuron* 2018; **99**: 64-82.e7.

48 Kabbani N, Olds JL. Does COVID19 Infect the Brain? If So, Smokers Might Be at a Higher Risk. *Mol Pharmacol* 2020; **97**: 351–353.

49 Zubair AS, McAlpine LS, Gardin T, Farhadian S, Kuruvilla DE, Spudich S. Neuropathogenesis and Neurologic Manifestations of the Coronaviruses in the Age of Coronavirus Disease 2019: A Review. *JAMA Neurol* 2020; **77**: 1018–1027.

50 Taquet M, Luciano S, Geddes JR, Harrison PJ. Bidirectional associations between COVID-19 and psychiatric disorder: retrospective cohort studies of 62□354 COVID-19 cases in the USA. *Lancet Psychiatry* 2021; **8**: 130–140.

51 Varatharaj A, Thomas N, Ellul MA, Davies NWS, Pollak TA, Tenorio EL *et al.* Neurological and neuropsychiatric complications of COVID-19 in 153 patients: a UK-wide surveillance study. *Lancet Psychiatry* 2020; **7**: 875–882.

52 Chen M, Reed RR, Lane AP. Chronic Inflammation Directs an Olfactory Stem Cell Functional Switch from Neuroregeneration to Immune Defense. *Cell Stem Cell* 2019; **25**: 501-513.e5.

53 Kishimoto-Urata M, Urata S, Kagoya R, Imamura F, Nagayama S, Reyna RA *et al.* Prolonged and extended impacts of SARS-CoV-2 on the olfactory neurocircuit. *Sci Rep* 2022; **12**: 5728.

54 Hasegawa-Ishii S, Imamura F, Nagayama S, Murata M, Shimada A. Differential Effects of Nasal Inflammation and Odor Deprivation on Layer-Specific Degeneration of the Mouse Olfactory Bulb. *eNeuro* 2020; **7**: ENEURO.0403-19.2020.

55 Hasegawa-Ishii S, Shimada A, Imamura F. Neuroplastic changes in the olfactory bulb associated with nasal inflammation in mice. *J Allergy Clin Immunol* 2019; **143**: 978-989.e3.

56 Yang K, Hua J, Etyemez S, Paez A, Prasad N, Ishizuka K *et al.* Volumetric alteration of olfactory bulb and immune-related molecular changes in olfactory epithelium in first episode psychosis patients. *Schizophr Res* 2021; **235**: 9–11.

57 Evgrafov OV, Armoskus C, Wrobel BB, Spitsyna VN, Souaiaia T, Herstein JS *et al.* Gene Expression in Patient-Derived Neural Progenitors Implicates WNT5A Signaling in the Etiology of Schizophrenia. *Biol Psychiatry* 2020. doi:10.1016/j.biopsych.2020.01.005.

58 Horiuchi Y, Kano S-I, Ishizuka K, Cascella NG, Ishii S, Talbot CC *et al.* Olfactory cells via nasal biopsy reflect the developing brain in gene expression profiles: utility and limitation of the surrogate tissues in research for brain disorders. *Neurosci Res* 2013; **77**: 247–250.

59 Kano S, Colantuoni C, Han F, Zhou Z, Yuan Q, Wilson A *et al.* Genome-wide profiling of multiple histone methylations in olfactory cells: further implications for cellular susceptibility to oxidative stress in schizophrenia. *Mol Psychiatry* 2013; **18**: 740–742.

60 Lavoie J, Gassó Astorga P, Segal-Gavish H, Wu YC, Chung Y, Cascella NG *et al.* The Olfactory Neural Epithelium As a Tool in Neuroscience. *Trends Mol Med* 2017; **23**: 100–103.

61 Takayanagi Y, Ishizuka K, Laursen TM, Yukitake H, Yang K, Cascella NG *et al.* From population to neuron: exploring common mediators for metabolic problems and mental illnesses. *Mol Psychiatry* 2021; **26**: 3931–3942.

62 Hasegawa Y, Namkung H, Smith A, Sakamoto S, Zhu X, Ishizuka K *et al.* Causal impact of local inflammation in the nasal cavity on higher brain function and cognition. *Neurosci Res* 2021; **172**: 110–115.

63 Lane AP, Turner J, May L, Reed R. A genetic model of chronic rhinosinusitis-associated olfactory inflammation reveals reversible functional impairment and dramatic neuroepithelial reorganization. *J Neurosci Off J Soc Neurosci* 2010; **30**: 2324–2329.

64 Saito A, Taniguchi Y, Rannals MD, Merfeld EB, Ballinger MD, Koga M *et al.* Early postnatal GABAA receptor modulation reverses deficits in neuronal maturation in a conditional neurodevelopmental mouse model of DISC1. *Mol Psychiatry* 2016; **21**: 1449–1459.

65 Leucht S, Samara M, Heres S, Davis JM. Dose Equivalents for Antipsychotic Drugs: The DDD Method. *Schizophr Bull* 2016; **42 Suppl 1**: S90-94.

66 Narayan S, McLean C, Sawa A, Lin SY, Rai N, Hipolito MS *et al.* Olfactory neurons obtained through nasal biopsy combined with laser-capture microdissection: a potential approach to study treatment response in mental disorders. *J Vis Exp JoVE* 2014. doi:10.3791/51853.

67 Mor E, Kano S-I, Colantuoni C, Sawa A, Navon R, Shomron N. MicroRNA-382 expression is elevated in the olfactory neuroepithelium of schizophrenia patients. *Neurobiol Dis* 2013; **55**: 1–10.

68 Andrews S. FastQC: a quality control tool for high throughput sequence data. 2010.http://www.bioinformatics.babraham.ac.uk/projects/fastqc.

69 Martin M. Cutadapt removes adapter sequences from high-throughput sequencing reads. *EMBnet.journal* 2011; **17**: 10–12.

70 Pertea M, Kim D, Pertea GM, Leek JT, Salzberg SL. Transcript-level expression analysis of RNA-seq experiments with HISAT, StringTie and Ballgown. *Nat Protoc* 2016; **11**: 1650–1667.

71 Love MI, Huber W, Anders S. Moderated estimation of fold change and dispersion for RNA-seq data with DESeq2. *Genome Biol* 2014; **15**: 550.

72 Leek JT, Johnson WE, Parker HS, Jaffe AE, Storey JD. The sva package for removing batch effects and other unwanted variation in high-throughput experiments. *Bioinformatics* 2012; **28**: 882–883.

73 Subramanian A, Tamayo P, Mootha VK, Mukherjee S, Ebert BL, Gillette MA *et al.* Gene set enrichment analysis: A knowledge-based approach for interpreting genome-wide expression profiles. *Proc Natl Acad Sci* 2005; **102**: 15545–15550.

74 Fabregat A, Jupe S, Matthews L, Sidiropoulos K, Gillespie M, Garapati P *et al.* The Reactome Pathway Knowledgebase. *Nucleic Acids Res* 2018; **46**: D649–D655.

75 MacArthur J, Bowler E, Cerezo M, Gil L, Hall P, Hastings E *et al.* The new NHGRI-EBI Catalog of published genome-wide association studies (GWAS Catalog). *Nucleic Acids Res* 2017; **45**: D896–D901.

76 Arnold SE, Smutzer GS, Trojanowski JQ, Moberg PJ. Cellular and molecular neuropathology of the olfactory epithelium and central olfactory pathways in Alzheimer's disease and schizophrenia. *Ann N Y Acad Sci* 1998; **855**: 762–775.

77 Pantazopoulos H, Boyer-Boiteau A, Holbrook EH, Jang W, Hahn C-G, Arnold SE *et al.* Proteoglycan abnormalities in olfactory epithelium tissue from subjects diagnosed with schizophrenia. *Schizophr Res* 2013; **150**: 366–372.

78 Smutzer G, Lee VM, Trojanowski JQ, Arnold SE. Human olfactory mucosa in schizophrenia. *Ann Otol Rhinol Laryngol* 1998; **107**: 349–355.

79 Abrams MT, Kaufmann WE, Rousseau F, Oostra BA, Wolozin B, Taylor CV *et al.* FMR1 gene expression in olfactory neuroblasts from two males with fragile X syndrome. *Am J Med Genet* 1999; **82**: 25–30.

80 Brown AS, Borgmann-Winter K, Hahn C-G, Role L, Talmage D, Gur R *et al.* Increased stability of microtubules in cultured olfactory neuroepithelial cells from individuals with schizophrenia. *Prog Neuropsychopharmacol Biol Psychiatry* 2014; **48**: 252–258.

81 English JA, Fan Y, Föcking M, Lopez LM, Hryniewiecka M, Wynne K *et al.* Reduced protein synthesis in schizophrenia patient-derived olfactory cells. *Transl Psychiatry* 2015; **5**: e663.

82 Féron F, Perry C, Hirning MH, McGrath J, Mackay-Sim A. Altered adhesion, proliferation and death in neural cultures from adults with schizophrenia. *Schizophr Res* 1999; **40**: 211–218.

83 Ghanbari HA, Ghanbari K, Harris PLR, Jones PK, Kubat Z, Castellani RJ *et al.* Oxidative damage in cultured human olfactory neurons from Alzheimer's disease patients. *Aging Cell* 2004; **3**: 41–44.

84 Girard SD, Devéze A, Nivet E, Gepner B, Roman FS, Féron F. Isolating nasal olfactory stem cells from rodents or humans. *J Vis Exp JoVE* 2011. doi:10.3791/2762.

85 Mackay-Sim A. Concise review: Patient-derived olfactory stem cells: new models for brain diseases. *Stem Cells Dayt Ohio* 2012; **30**: 2361–2365.

86 Matigian N, Abrahamsen G, Sutharsan R, Cook AL, Vitale AM, Nouwens A *et al.* Disease-specific, neurosphere-derived cells as models for brain disorders. *Dis Model Mech* 2010; **3**: 785–798.

87 Rhie SK, Schreiner S, Witt H, Armoskus C, Lay FD, Camarena A *et al.* Using 3D epigenomic maps of primary olfactory neuronal cells from living individuals to understand gene regulation. *Sci Adv* 2018; **4**: eaav8550.

88 Solís-Chagoyán H, Calixto E, Figueroa A, Montaño LM, Berlanga C, Rodríguez-Verdugo MS *et al.* Microtubule organization and L-type voltage-activated calcium current in olfactory neuronal cells obtained from patients with schizophrenia and bipolar disorder. *Schizophr Res* 2013; **143**: 384–389.

89 Wolozin B, Lesch P, Lebovics R, Sunderland T. A.E. Bennett Research Award 1993. Olfactory neuroblasts from Alzheimer donors: studies on APP processing and cell regulation. *Biol Psychiatry* 1993; **34**: 824–838.

90 Merritt CR, Ong GT, Church SE, Barker K, Danaher P, Geiss G *et al.* Multiplex digital spatial profiling of proteins and RNA in fixed tissue. *Nat Biotechnol* 2020; **38**: 586–599.

Table 1. Demographic statistics of study cohort.
Significant results are highlighted in bold. Abbreviations: SD, standard deviation; Y, yes; N, no; AA, African American.

All subjects			
	Controls (n=89)	**Patients (n=95)**	**p-value**
Age (mean/SD)	23.53 / 3.89	22.06 / 4.41	**0.02**
Gender (Male/Female)	40 / 49	70 / 25	**1.32E-04**
Race (AA/Caucasian/Asian/others)	56 / 25 / 2 / 6	45 / 34 / 6 / 10	**4.88E-02**
Tobacco use (Y/N)	3 / 86	24 / 71	**6.73E-05**

Subjects with RNA-Seq data			
	Controls (n=59)	**Patients (n=45)**	**p-value**
Age (mean/SD)	23.33 +- 3.25	22.71 +- 3.88	0.38
Gender (Male/Female)	31 / 28	31 / 14	0.14
Race (AA/Caucasian/Asian/others)	37 / 16 / 2 / 4	26 / 14 / 2 / 3	0.76
Tobacco use (Y/N)	2 / 57	8 / 37	**0.03**

Figure legends

Figure 1. Structural alterations in the olfactory bulb (OB) in inducible olfactory epithelium inflammation (IOI) mice.

(A) The size of OB: left panel: dorsal views of the OBs, and schematic diagram of the OB measurement methods; right panel: quantification of the length and width in OB (n = 6 mice per condition).

(**B)** DAPI staining of OB (white): left panel: representative image of OB coronal section. Scale bar, 500 μm; middle panel: schematic diagram of OB layers in the coronal section; right panel: quantification of each area as % of total OBs area. GL, glomerular layer; EPL, external plexiform layer; MCL, mitral cell layer; IPL, internal plexiform layer; GCL, granule cell layer. (n = 10 mice per condition).

(**C)** Immunohistochemistry with antibody against OMP (green), VGlut2 (red), CCK8 (red), and PGP9.5 (red) with DAPI staining in the GL: left panel: representative images of the GL. Scale bar, 50 μm; right panel: quantification of the signal intensity of OMP, VGlut2, CCK8, and PGP9.5 as % of control (n = 6-12 mice per condition).

***$p < 0.001$, **$p < 0.01$, *$p < 0.05$, determined by t-test. Data are presented as the mean ± s.e.m.

Figure 2. Volumetric alterations in the olfactory bulb (OB) in first episode psychosis (FEP) patients.

(A) Representative image of OB in T2-weighted images at 3 Tesla

(B) Boxplot of total OB volumes between FEP patients and healthy controls.

(C) Boxplot of right OB volumes between FEP patients and healthy controls.

(D) Boxplot of left OB volumes between FEP patients and healthy controls.

***$p < 0.001$, **$p < 0.01$, *$p < 0.05$, determined by ANCOVA

Figure 3. Correlation between OB volumes and the expressional profiles of immune-related transcription factors up-regulated by olfactory epithelium inflammation (IOI immune genes) in first episode psychosis (FEP) patients.

(A) Dot pot of the first principal component (PC1) of the expressional levels of IOI immune genes *versus* the mean expressional levels of IOI immune genes.

(B) Dot pot of PC1 of the expressional levels of IOI immune genes *versus* total OB volume.

(C) Dot pot of PC1 of the expressional levels of IOI immune genes *versus* right OB volume.

(D) Dot pot of PC1 of the expressional levels of IOI immune genes *versus* left OB volume.

***$p < 0.001$, **$p < 0.01$, *$p < 0.05$, determined by partial correlation analysis.

Figure 1.

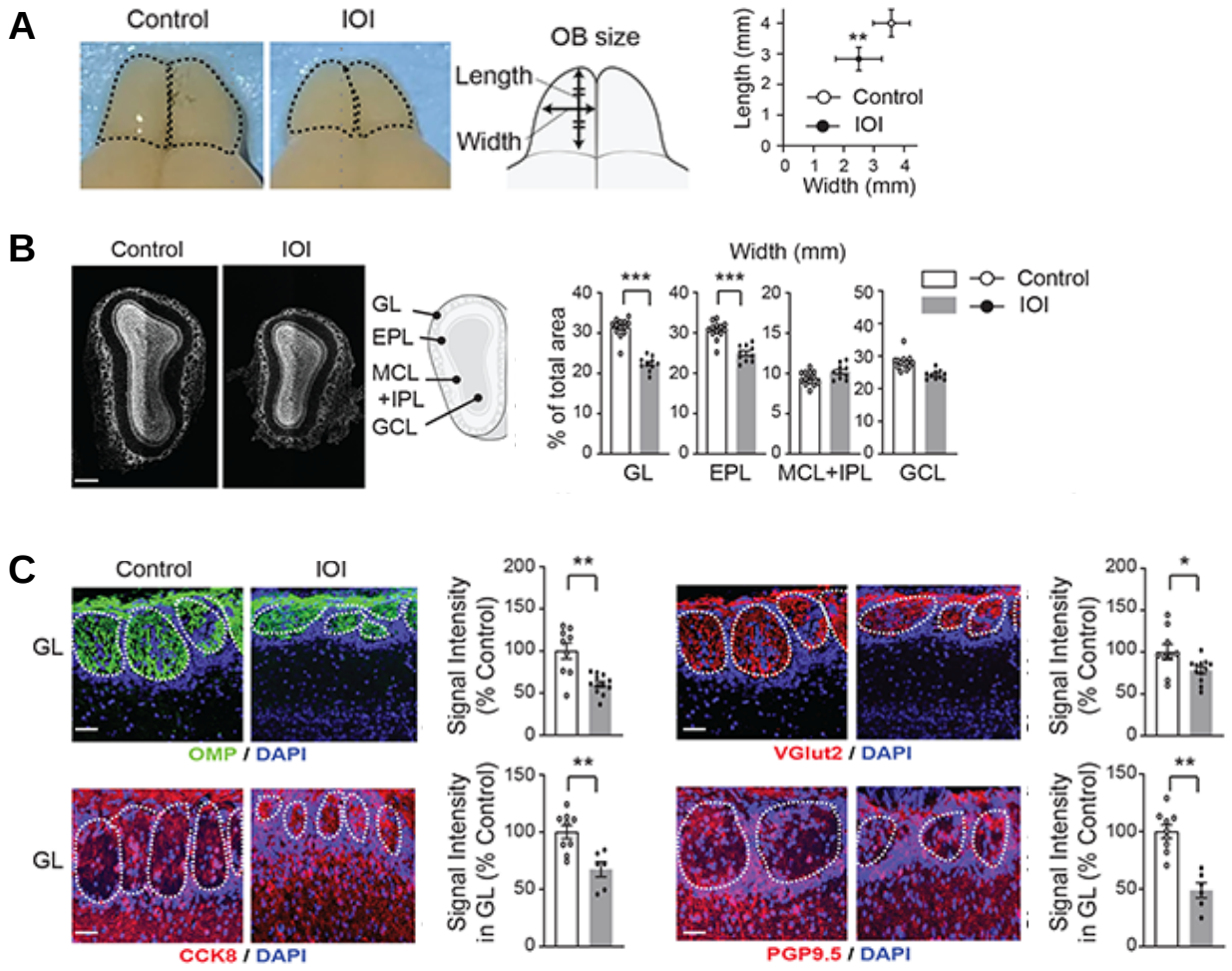
A
Control
IOI
OB size
Length
Width
Length (mm)
Width (mm)
Control
IOI
B
Control
IOI
GL
EPL
MCL
+IPL
GCL
Width (mm)
% of total area
GL
EPL
MCL+IPL
GCL
C
Control
IOI
GL
OMP / DAPI
Signal Intensity (% Control)
VGlut2 / DAPI
CCK8 / DAPI
Signal Intensity in GL (% Control)
PGP9.5 / DAPI

Figure 2.

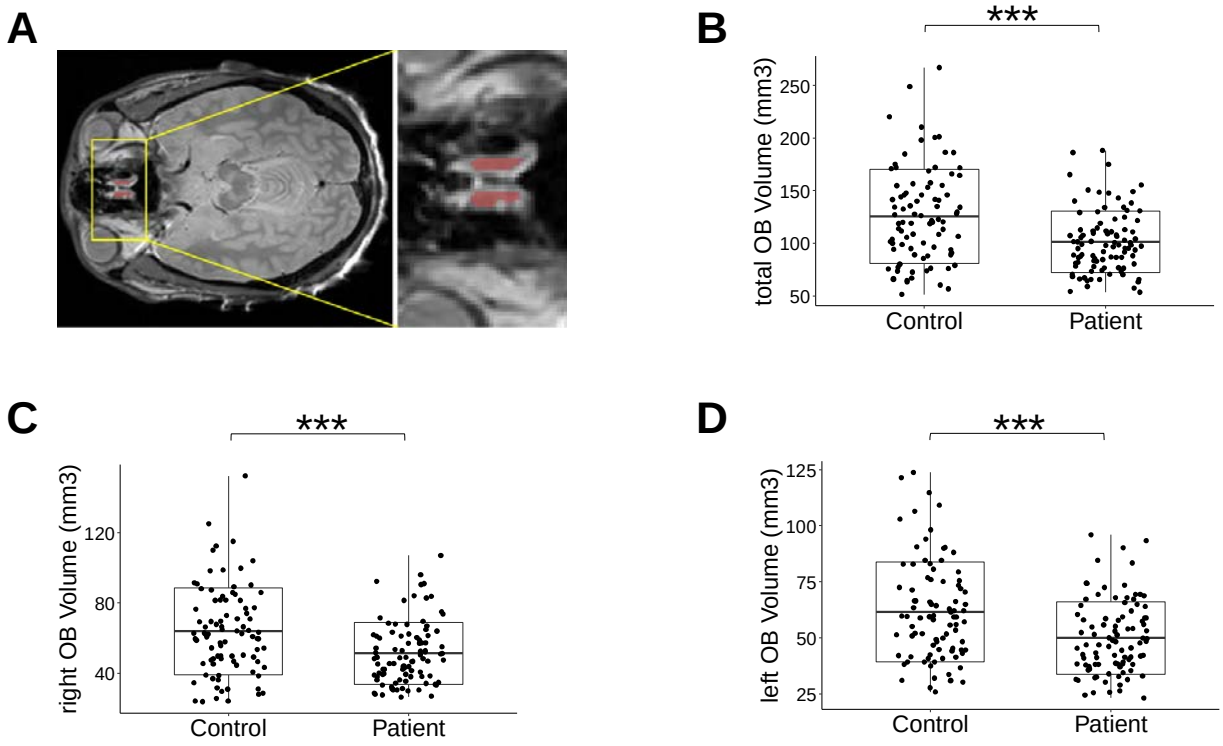
A
B
***
total OB Volume (mm3)
250
200
150
100
50
Control
Patient
C
***
right OB Volume (mm3)
120
80
40
Control
Patient
D
***
left OB Volume (mm3)
125
100
75
50
25
Control
Patient

Figure 3.

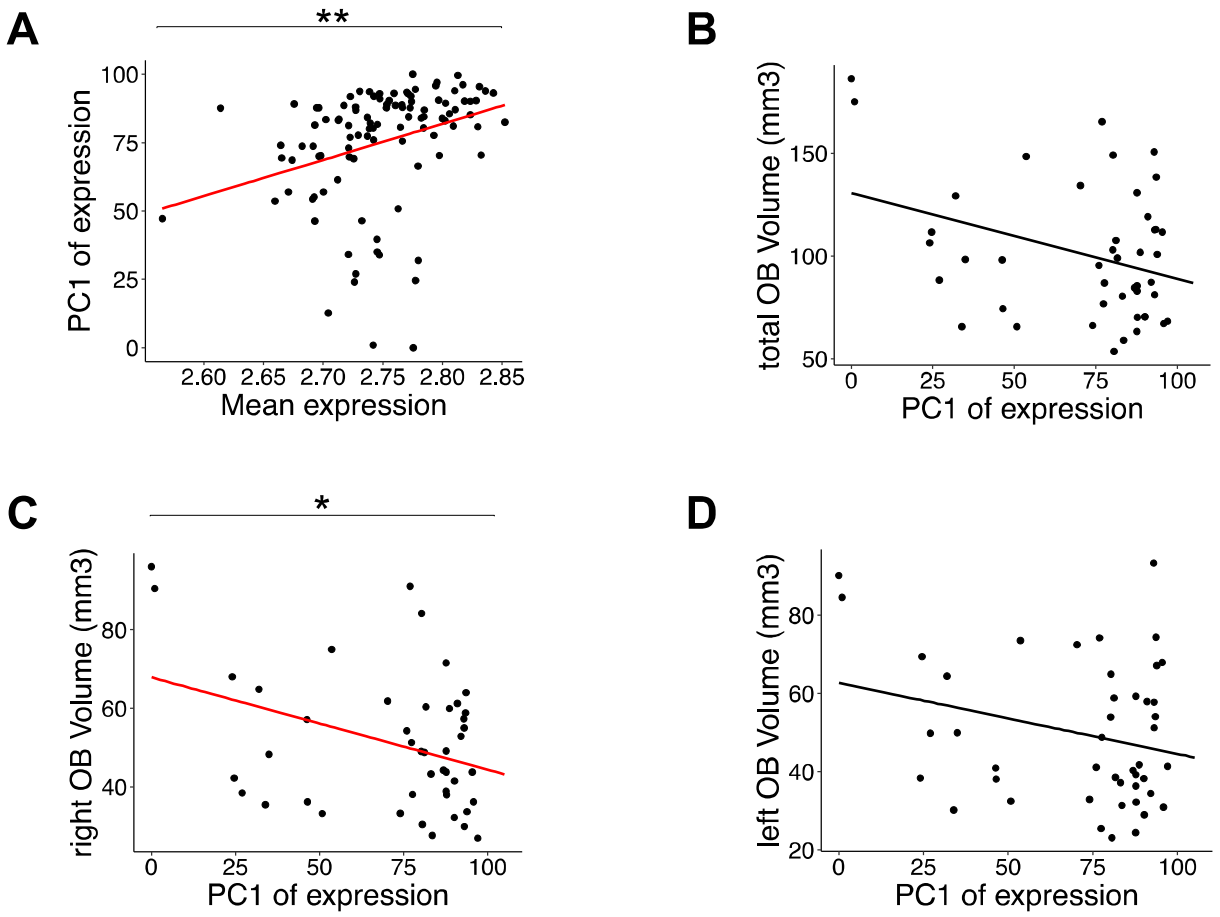
A
**
PC1 of expression
100
75
50
25
0
2.60 2.65 2.70 2.75 2.80 2.85
Mean expression
B
total OB Volume (mm3)
150
100
50
0 25 50 75 100
PC1 of expression
C
*
right OB Volume (mm3)
80
60
40
0 25 50 75 100
PC1 of expression
D
left OB Volume (mm3)
80
60
40
20
0 25 50 75 100
PC1 of expression